Chinese Journal of Natural Medicines

Structurally diverse sesquiterpenoids with anti-MDR cancer activity from *Penicillium roqueforti*

Shuyuan Mo, Nanjin Ding, Zhihong Huang, Jun Yao, Weiguang Sun, Jianping Wang, Yonghui Zhang, Zhengxi Hu

Citation: Shuyuan Mo, Nanjin Ding, Zhihong Huang, Jun Yao, Weiguang Sun, Jianping Wang, Yonghui Zhang, Zhengxi Hu, Structurally diverse sesquiterpenoids with anti-MDR cancer activity from *Penicillium roqueforti*, Chinese Journal of Natural Medicines, 2025, 23(4), 504-512. doi: 10.1016/S1875-5364(25)60857-0.

View online: https://doi.org/10.1016/S1875-5364(25)60857-0

Chinese Journal of Natural Medicines 23 (2025) 504-512

Contents lists available at ScienceDirect

Chinese Journal of Natural Medicines

journal homepage: www.cjnmcpu.com/

Original article

Structurally diverse sesquiterpenoids with anti-MDR cancer activity from *Penicillium roqueforti*

Shuyuan Mo[a,c,Δ], Nanjin Ding[a,Δ], Zhihong Huang[a], Jun Yao[a], Weiguang Sun[a], Jianping Wang[a,*], Yonghui Zhang[a,*], Zhengxi Hu[a,b,*]

[a] *Hubei Key Laboratory of Natural Medicinal Chemistry and Resource Evaluation, School of Pharmacy, Tongji Medical College, Huazhong University of Science and Technology, Wuhan 430030, China*

[b] *Hubei Shizhen Laboratory, Wuhan 430061, China*

[c] *Department of Pharmacy, Renmin hospital of Wuhan University, Wuhan 430060, China*

ARTICLE INFO

Article history:
Received 26 February 2024
Revised 13 May 2024
Accepted 4 June 2024
Available online 20 April 2025

Keywords:
Penicillium roqueforti
Sesquiterpenoids
Nor-sesquiterpenoids
Anti-MDR cancer activity

ABSTRACT

Five novel *nor*-eremophilane-type sesquiterpenoids, peniroqueforins E–H and J (**1**–**4** and **7**), two new eremophilane-type sesquiterpenoids, peniroqueforins I and K (**5** and **8**), and a new eudesmane-type sesquiterpenoid, peniroqueforin L (**9**), along with four known compounds (**6** and **10**–**12**), were isolated and characterized from fungus *Penicillium roqueforti* (*P. roqueforti*). The structures and absolute configurations of these compounds were determined through comprehensive spectroscopic analyses, electronic circular dichroism (ECD) data analyses, and single-crystal X-ray diffraction methods. The anti-multi-drug resistance (MDR) cancer activity of these compounds was evaluated using SW620/Ad300 cells. Notably, the half maximal inhibitory concentration (IC_{50}) value of paclitaxel (PTX) combined with **1** in SW620/Ad300 cells was 50.36 nmol·L^{-1}, which was 65-fold more potent than PTX alone (IC_{50} 3.26 μmol·L^{-1}). Subsequent molecular docking studies revealed an affinity between compound **1** and P-glycoprotein (P-gp), suggesting that this *nor*-eremophilane-type sesquiterpenoid (**1**) could serve as a potential lead for MDR reversal in cancer cells through P-gp inhibition.

1. Introduction

According to estimates from the World Health Organization (WHO), approximately 18.1 million new cancer cases and 9.6 million cancer-related deaths occurred globally in 2018[1–3]. While chemotherapy remains the primary strategy for treating various types of cancer, multi-drug resistance (MDR) continues to be a significant obstacle leading to chemotherapy failure[4–7]. Over recent years, researchers have identified the P-glycoprotein (P-gp) pump as a major contributing factor to MDR[4–5]. Consequently, a range of P-gp inhibitors has been developed, including verapamil, cyclosporine analogs, and tariquidar[8]. However, these drugs are still specifically recognized and excreted by the P-gp pump, limiting their clinical applications[9]. Therefore, the pursuit of more potent and selective lead compounds from microorganisms presents a promising approach to overcoming MDR in cancer.

Over recent decades, fungi have emerged as a primary source for novel drug discovery, owing to their remarkable capacity to synthesize natural molecules with intriguing chemical structures and potential bioactivities[10–14]. In our ongoing quest to identify structurally unique and bioactive natural products from soil-derived fungi, we have concentrated on the fungus *Penicillium roqueforti* (*P. roqueforti*), isolated from the root soil of *Hypericum beanii* collected in the Shennongjia Forestry District. This investigation yielded a total of 12 compounds, comprising five new *nor*-eremophilane-type sesquiterpenoids (**1**–**4** and **7**), two new eremophilane-type sesquiterpenoids (**5** and **8**), and one new eudesmane-type sesquiterpenoid (**9**). All compounds were subjected to evaluation for anti-MDR cancer activity in SW620/Ad300 cells. This paper presents the isolation, structural elucidation, and bioactivity assessments of these compounds (Fig. 1).

2. Results

Compound **1** was isolated as a yellow needle crystal. The molecular formula, $C_{14}H_{16}O_4$, was determined by high-resolution electrospray ionization mass spectroscopy (HR-ESI-MS), which showed an ion peak at *m/z* 271.0940 ([M + Na]$^+$, Calcd. for 271.0941), indicating seven degrees of unsaturation. The ^{1}H and ^{13}C nuclear magnetic resonance (NMR) spectra, along with the HSQC spectrum, revealed one doublet methyl (δ_H 1.18) and two singlet methyls (δ_H 2.10 and 1.39), four olefinic protons (δ_H 6.54, 6.27, 6.18, and 6.15), and two methines (δ_H 5.47, and 2.07). Analysis of the DEPT and ^{13}C NMR data (Table 1) of **1** identified fourteen carbon resonances including three methyls (δ_C 24.5, 20.8, and 11.8), six methines (δ_C 132.5, 131.1, 124.6, 124.0, 71.3, and 39.7), and five non-protonated carbons (δ_C 183.5, 172.3, 164.6, 148.8, and 42.4). These data suggested that **1** possessed a bicyclic eremophilane sesquiterpenoid skeleton. Comparison of the ^{1}H

* Corresponding author.
E-mail addresses: jpwang1001@163.com (J. Wang); zhangyh@mails.tjmu.edu.cn (Y. Zhang); hzx616@126.com (Z. Hu)
Δ These authors contributed equally to this work.

https://doi.org/10.1016/S1875-5364(25)60857-0

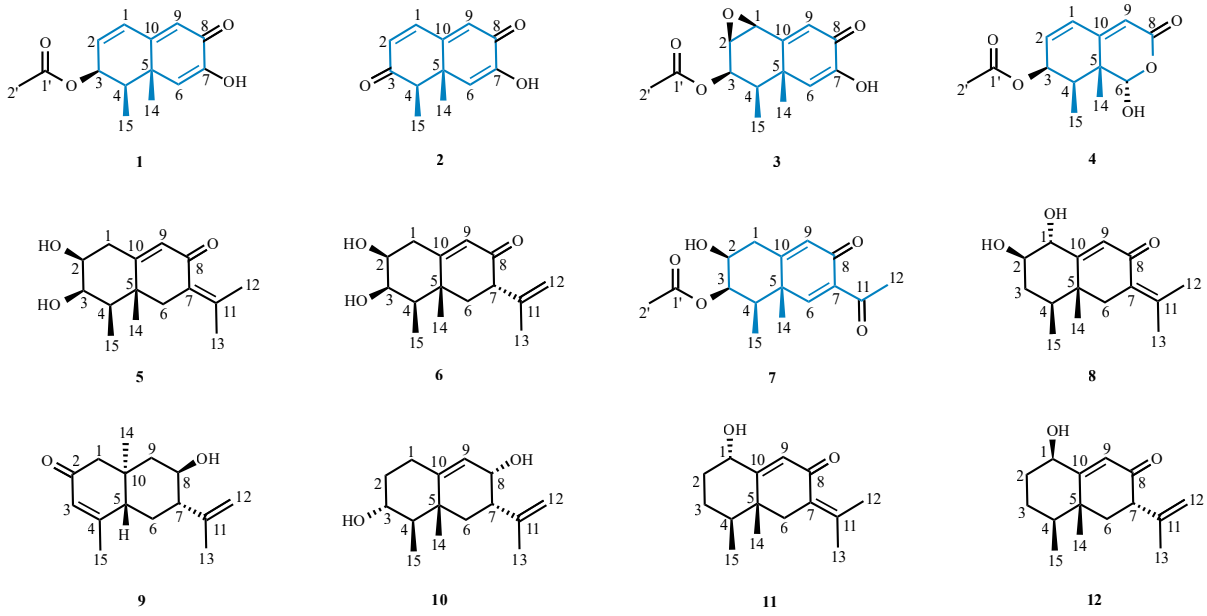

Fig. 1 Structures of compounds **1**–**12**.

and ^{13}C NMR data (Table 1) of **1** with the known compound 3*β*-(acetyloxy)-7-hydroxynoreremophila-6,9-dien-8-one [15] further indicated that compound **1** was also a 11,12,13-tri-*nor*-sesquiterpenoid derivative, differing in a substituted double bond at C-1 and C-2, as evidenced by the ^{1}H–^{1}H correlation spectroscopy (COSY) cross-peaks of H-1/H-2/H-3. The nuclear Overhauser effect spectroscopy (NOESY) spectrum (Fig. 3) showed correlations of H_3-14 (δ_H 1.39) with H-6 (δ_H 6.27) and of H_3-15 (δ_H 1.18) with H-6 (δ_H 6.27), indicating that H-6, H_3-14, and H_3-15 were on the same side. The absolute configuration was determined by single-crystal X-ray diffraction analysis using Cu K*α* radiation (Fig. 4) [Flack parameter = 0.13(7), Cambridge Crystallographic Data Centre (CCDC) 2304403]. Thus, the absolute configuration of **1** was unambiguously confirmed as 3*S*,4*R*,5*R*, and the compound was named as peniroqueforin E.

Compound **2** exhibited a molecular formula of $C_{12}H_{12}O_3$, as determined by the HR-ESI-MS peak at *m/z* 227.0688 $[M + Na]^+$. The analogous ^{1}H and ^{13}C NMR data (Table 1) indicated that compounds **1** and **2** shared an identical tri-*nor*-eremophilane sesquiterpenoid skeleton, with the notable distinction being the absence of an acetyl group and the presence of a keto carbonyl group at C-3 in **2**. The NOESY data of **2** closely resembled those of **1**, suggesting equivalent relative configurations for C-4 and C-5. Considering the biosynthetic pathway and the nearly identical electronic circular dichroism (ECD) patterns of **2** and **1** (Fig. 5), the absolute configuration of **2** was established as 4*R*,5*R*. Consequently, the structure of **2** was elucidated and designated as peniroqueforin F.

Compound **3**, isolated as a yellow needle crystal, exhibited a molecular formula of $C_{14}H_{16}O_5$ as determined *via* its HR-ESI-MS data. Comprehensive analysis of the NMR data (Table 1) of **1** and **3** indicated that both compounds were structural analogues. The primary distinction was attributed to the presence of a 1,2-epoxy group in **3**, evidenced by the most significant chemical shift differences between **1** and **3**. The ^{13}C NMR data observed at C-1 and C-2 in **1** and **3** shifted from δ_C 131.1 and 132.5 to δ_C 57.0 and 56.1, respectively. The NOESY (Fig. 3) correlations from H_3-15 (δ_H 1.15) and H_3-14 (δ_H 1.40) to H-6 (δ_H 6.19) suggested their positioning in the same orientations. A high-quality crystal of **3** was obtained through repeated recrystallization from MeOH–H_2O (20∶1) and subsequently subjected to single-crystal X-ray diffraction analysis with Cu K*α* (Fig. 4) [Flack parameter = 0.12(8), CCDC 2304404]. This analysis enabled the assignment of the absolute configuration as 1*S*,2*S*,3*R*,4*R*,5*R*, and the compound was designated as peniroqueforin G.

Compound **4** was isolated as a yellow block crystal with the molecular formula $C_{13}H_{16}O_5$, was determined by the ^{13}C NMR and HR-ESI-MS data analyses, indicating six degrees of unsaturation. Analysis of the 1D NMR data (Table 1) of **4** suggested it was a derivative of septeremophilane A[16], featuring a 7,11,12,13-tetra-*nor*-sesquiterpenoid skeleton. The primary difference was the replacement of the 6-methylocta-2,4-dienoyl moiety at C-3 in septeremophilane A with an acetyl group in **4**, confirmed by the key heteronuclear multiple bond correlation (HMBC) from H_3-2'

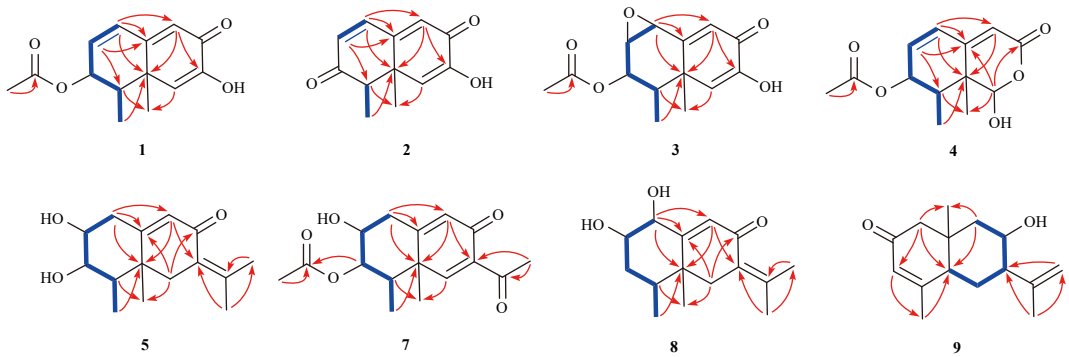

Fig. 2 Key ^{1}H–^{1}H COSY (blue lines) and HMBC (red arrows) correlations of **1**–**5** and **7**–**9**.

Table 1 ^{1}H and ^{13}C NMR spectroscopic data (δ in ppm, J in Hz) for compounds **1**–**4**.

No.	1		2		3		4	
	$\delta_C^{a,e}$	$\delta_H^{a,c}$	$\delta_C^{a,e}$	$\delta_H^{a,c}$	$\delta_C^{b,e}$	$\delta_H^{b,c}$	$\delta_C^{b,f}$	$\delta_H^{b,d}$
1	131.1 CH	6.54 d (9.8)	143.5 CH	7.39 d (9.9)	57.0 CH	3.78 d (3.8)	129.3 CH	6.36 d (9.8)
2	132.5 CH	6.18 dd (9.8, 5.0)	132.3 CH	6.27 d (9.9)	56.1 CH	3.91 dd (4.8, 3.8)	133.5 CH	6.31 dd (9.8, 5.0)
3	71.3 CH	5.47 t (5.0)	200.7 C		70.2 CH	5.16 dd (5.6, 4.8)	69.8 CH	5.38 t (5.0)
4	39.7 CH	2.07 m	52.2 CH	2.60 q (7.1)	43.6 CH	1.81 qd (7.1, 5.6)	33.7 CH	2.52 qd (7.1, 5.0)
5	42.4 C		46.3 C		42.6 C		39.5 C	
6	124.0 CH	6.27 s	125.5 CH	6.36 s	125.0 CH	6.19 s	100.0 CH	5.53 s
7	148.8 C		149.8 C		146.1 C			
8	183.5 C		182.9 C		180.4 C		163.7 C	
9	124.6 CH	6.15 s	128.1 CH	6.53 s	126.4 CH	6.61 s	114.8 CH	5.82 s
10	164.6 C		161.5 C		163.3 C		155.5 C	
14	24.5 CH_3	1.39 s	23.7 CH_3	1.22 s	20.8 CH_3	1.40 s	18.9 CH_3	1.32 s
15	11.8 CH_3	1.18 d (7.1)	8.4 CH_3	1.29 d (7.1)	11.6 CH_3	1.15 d (7.1)	10.1 CH_3	1.05 d (7.1)
1'	172.3 C				170.8 C		170.7 C	
2'	20.8 CH_3	2.10 s			20.9 CH_3	2.16 s	21.1 CH_3	2.09 s

[a]In methanol-d_4. [b]In chloroform-d. [c]Recorded at 400 MHz. [d]Recorded at 600 MHz. [e]Recorded at 100 MHz. [f]Recorded at 150 MHz. "m" means overlapped or multiplet with other signals.

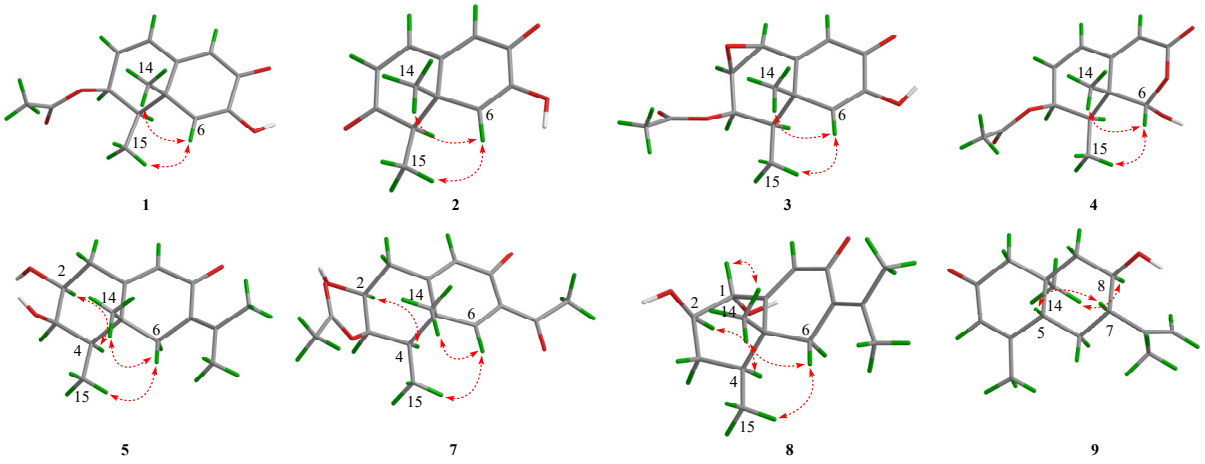

Fig. 3 Key ROESY/NOESY correlations of compounds **1**–**5** and **7**–**9**.

(δ_H 2.09) to C-1' (δ_C 170.7) (Fig. 2). The ROESY data (Fig. 3) were comparable to those of **1**. Single-crystal X-ray diffraction analysis with Cu Kα (Fig. 4) yielded a Flack parameter of 0.14(10), confirming the absolute configuration of **4** as 3*S*,4*R*,5*R*,6*S* (CCDC 2304405). Consequently, this compound was characterized and designated as peniroqueforin H.

Compound **5** was isolated as a yellow block crystal, with the molecular formula $C_{15}H_{22}O_3$ (five degrees of unsaturation), as determined by its HR-ESI-MS and NMR data (Table 2). Comparison of the NMR data of **5** and **1** revealed that they had the similar eremophilane sesquiterpenoid skeleton. The key NOESY correlations (Fig. 3) from H_3-15 (δ_H 1.17) and H_3-14 (δ_H 1.14) to H-6β (δ_H 2.97) and from H-4 (δ_H 1.51) to H-2 (δ_H 3.62) suggested that H-6β, H_3-14, and H_3-15 were on the same side with β-orientations, while both H-2 and H-4 were on the opposite side. The absolute configuration of **5** was established as 2*S*,3*R*,4*R*,5*R* through single-crystal X-ray diffraction analysis with Cu Kα (Fig. 4) [Flack parameter = 0.07(7), CCDC 2304406]. This compound was subsequently named as peniroqueforin I.

Compound **7** was isolated as a yellow amorphous powder, with a molecular formula of $C_{16}H_{20}O_5$, as determined by HR-ESI-MS and NMR data. The ^{1}H and ^{13}C NMR spectra (Table 2) of **7** closely resembled those of the known compound 1β-acetoxy-6,9-dien-8-oxoeremophil-11-*nor*-11-ketone [17], indicating a shared core skeleton. However, notable differences were observed: (1) In **7**, an acetyl group[16], was linked to C-3 rather than C-1, as evidenced by the HMBC correlation from H-3 (δ_H 5.28) to C-1' (δ_C 173.6) (Fig. 2); (2) An additional hydroxy group was present at C-2 in compound **7**. These observations established the planar structure of compound **7**. Analysis of key ROESY correlations revealed similarities to those of **5**, suggesting analogous relative configurations. The experimental ECD spectra (Fig. 5) for **5** and **7** showed good agreement, confirming the absolute configuration of **7** as 2*S*,3*R*,4*R*,5*R*. Consequently, the structure of **7** was elucidated and designated as peniroqueforin J.

Compound **8** was isolated as a yellow amorphous powder. Its molecular formula was determined by HR-ESI-MS, which showed an ion peak at *m/z* 273.1467 ([M + Na]$^+$, Calcd. for 273.1461), corresponding to a molecular formula of $C_{15}H_{22}O_3$ with five degrees of unsaturation. The NMR data (Table 2) of **8** were similar to those of rhizoperemophilane B [18], indicating structural similarity. ROESY correlations (Fig. 3) between H_3-15 (δ_H 1.01)/H-6β (δ_H 2.49), H_3-14 (δ_H 1.03)/H-6β, and H_3-14 (δ_H 1.03)/H-1 (δ_H 3.99) suggested that H_3-15, H_3-14, H-6β, and H-1 were β-oriented. Conversely, the NOESY correlation between H-4 (δ_H 1.60) and H-2 (δ_H 3.41) indicated their opposite orientation.

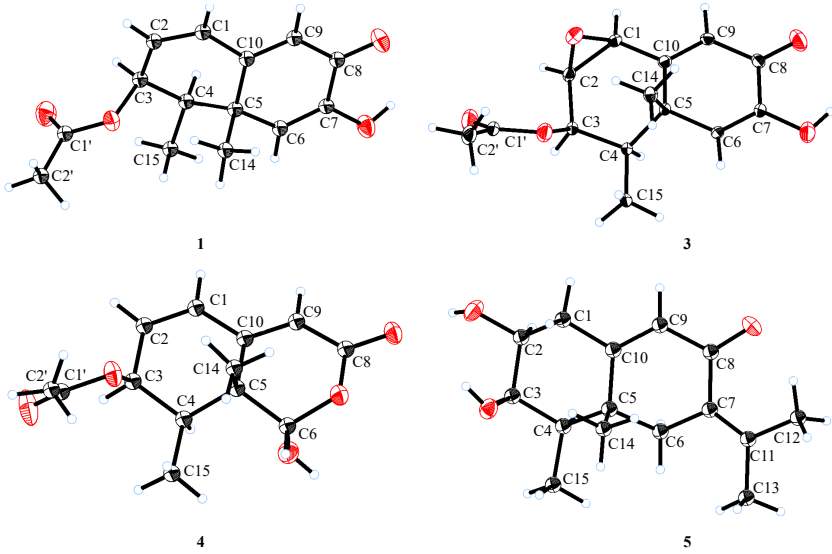

Fig. 4 ORTEP drawings of compounds **1** and **3**–**5**.

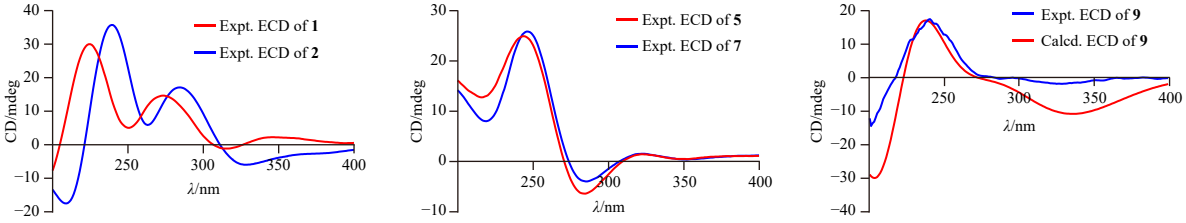

Fig. 5 Comparison of the experimental ECD curves of **1**–**2**, **5**, and **7** and calculated ECD spectrum of **9**.

Furthermore, a large $^{3}J_{H\text{-}3/H\text{-}4}$ value of 10.8 Hz in **8** demonstrated a *trans* relationship between H-1 and H-2[15]. Based on the biosynthetic pathway and the aforementioned spectroscopic data, the absolute configuration of **8** was established 1*R*,2*R*,4*S*,5*R*. Consequently, compound **8** was characterized and designated as peniroqueforin K.

Compound **9** was isolated as a colorless oil. Its molecular formula was determined as $C_{15}H_{22}O_2$ by through HR-ESI-MS analysis, indicating five degrees of unsaturation. The ^{1}H and ^{13}C NMR data (Table 2) of **9** closely resembled those of the known compound stigolone [19]. The key distinction was the hydroxylation of C-8 in **9**, whereas both C-8 and C-9 were hydroxylated in stigolone. This difference was evidenced by the most significant chemical shift variations between **9** and stigolone observed at C-8 and C-9, which shifted from δ_C 67.8 and 49.3 to δ_C 72.5 and 75.8, respectively. The NOESY cross-peaks (Fig. 3) of H_3-14 (δ_H 0.94)/H-8 (δ_H 3.80) indicated their positioning on the same side. The large spin-spin coupling ($^{3}J_{H\text{-}7/H\text{-}8}$ = 10.9 Hz) revealed their opposite orientation. Additionally, the NOESY cross-peak of H-5 (δ_H 2.59)/ H-7 (δ_H 2.14) confirmed their positioning on the same side. Consequently, the relative configuration was established as shown in Fig. 3. The absolute configuration of **9** was determined as 5*R*,7*S*,8*R*,10*R* by comparing the experimental and computed ECD curves (Fig. 5). Thus, the structure of **9** was elucidated and named as peniroqueforin L.

Four previously reported eremophilane-type sesquiterpenoids were identified through comparison of their spectroscopic data with literature values. These compounds include 1-dehydroxy guignarderemophilane C (**6**) [20], dihydropetasol (**10**) [21], 1β-hydroxy dehydrofukinones (**11**) [22], and 1-hydroxy-eremophila-9,11-dien-8-one (**12**) [23].

Compounds (**1**–**12**) were initially evaluated for their anti-tumor activity in MCF-7, HepG2, and C4-2B cells (Table 3). The results indicated that compounds **1**–**12** exhibited no significant cytotoxicity in these cancer cells, with low inhibitory values at 20 μmol·L^{-1}. However, when combined with paclitaxel (PTX), compound **1** demonstrated a significant inhibitory effect on the survival ratio of multi-drug resistant (MDR) SW620/Ad300 cells. As illustrated inFig. 6 and Table 3, the half maximal inhibitory concentration (IC_{50}) values of PTX without and with **1** in SW620/Ad300 cells were 3.26 μmol·L^{-1} and 50.36 nmol·L^{-1}, respectively, indicating a 65-fold reduction in PTX resistance. Additionally, the IC_{50} values of PTX without and with **1** in non-drug resistant parental SW620 cells decreased from 2.62 to 0.38 nmol·L^{-1}, suggesting 6.9-fold reversal index.

Motivated by the aforementioned intriguing results, we investigated the impact of **1** alone and in combination with PTX on the cell proliferation and cell cycle dynamics of SW620/Ad300 cells using colony formation assays and cell cycle analysis. Compound **1** significantly enhanced PTX's inhibitory effect on SW620/Ad300 cell colony formation, exhibiting greater efficacy than **1** or PTX alone (Figs. 7A–7B). Furthermore, cell cycle analysis revealed that the combination of **1** and PTX significantly reduced the proportion of cells in the G_0/G_1phase while increasing the frequency in the G_2/Mphase (Figs. 7C–7D). This outcome aligns with PTX's known mechanism of impeding mitosis, suggesting that **1** plays a role in reversing PTX resistance in SW620/Ad300 cells.

Rhodamine 123 (Rho 123) serves as a specific P-gp probe, demonstrating P-gp transport capacity through its fluorescence accumulation in cells [24–26]. The Rho 123 accumulation assay revealed that higher doses of **1** corresponded to increased intracellular Rho 123 percentage in SW620/Ad300 cells (Fig. 8A), indicating that **1** inhibited P-gp efflux function. To elucidate the potential binding model of **1** with P-gp, molecular modeling was conducted using the zosuquidar and human-mouse chimeric P-gp complex as the docking template (Fig. 8B). Compound **1** was primarily stabilized within the binding cavity in the transmem-

Table 2 ^{1}H and ^{13}C NMR spectroscopic data (δ in ppm, J in Hz) for compounds **5** and **7**–**9**.

No.	5		7		8		9	
	δ_C [a,e]	δ_H [a,c]	δ_C [a,f]	δ_H [a,d]	δ_C [a,f]	δ_H [a,d]	δ_C [a,e]	δ_H [a,d]
1	36.5 CH_2	2.78 dd (14.0, 2.0); 2.28 dd (14.0, 4.6)	37.4 CH_2	2.86 dd (12.3, 4.8); 2.56 dd (12.3, 1.6)	75.2 CH	3.99 dd (10.8, 2.1)	55.0 CH_2	2.35 dd (16.2, 1.2); 2.23 dd (16.2, 1.2)
2	72.7 CH	3.62 ddd (12.3, 4.6, 2.0)	72.1 CH	3.72 ddd (12.3, 4.8, 3.2)	75.4 CH	3.41 ddd (10.8, 9.6, 4.8)	201.7 C	
3	75.1 CH	3.76 t (2.3)	76.2 CH	5.28 t (3.2)	38.4 CH_2	1.84 ddd (12.9, 4.8, 2.9); 1.54 dd (12.9, 10.8)	127.2 CH	5.87 s
4	44.9 CH	1.51 qd (7.1, 2.3)	40.6 CH	1.79 qd (7.1, 3.2)	40.5 CH	1.60 ddd (12.9, 7.1, 2.9)	166.3 C	
5	42.0 C		44.4 C		43.2 C		48.3 CH	2.59 dtd (12.7, 3.1, 1.4)
6	42.9 CH_2	2.97 d (13.3); 2.03 d (13.3)	160.1 CH	7.63 s	42.4 CH_2	2.94 d (13.9); 2.19 d (13.9)	30.1 CH_2	1.98 dt (13.5, 3.1); 1.54 dt (13.5, 12.7)
7	128.9 C		137.6 C		128.6 C		56.0 CH	2.14 ddd (12.7, 10.5, 4.2)
8	194.1 C		185.1 C		194.2 C		67.8 CH	3.80 td (10.5, 4.5)
9	127.5 CH	5.77 s	127.3 CH	6.22 s	124.5 CH	6.19 s	49.3 CH_2	1.84 dd (11.8, 4.5); 1.43 t (11.8)
10	170.2 C		166.6 C		170.3 C		39.9 C	
11	145.7 C		200.9 C		145.1 C		147.9 C	
12	22.9 CH_3	2.07 s	30.7 CH_3	2.48 s	22.8 CH_3	2.06 s	112.8 CH_2	4.87 m
13	22.4 CH_3	1.88 s			22.3 CH_3	1.90 s	19.9 CH_3	1.80 s
14	19.3 CH_3	1.14 s	20.2 CH_3	1.39 s	17.4 CH_3	1.03 s	17.9 CH_3	0.94 s
15	12.4 CH_3	1.17 d (7.1)	12.3 CH_3	1.18 d (7.1)	15.2 CH_3	1.01 d (7.1)	22.3 CH_3	1.94 s
1′			172.6 C					
2′			21.0 CH_3	2.18 s				

[a]In methanol-d_4. [b]In chloroform-d. [c]Recorded at 400 MHz. [d]Recorded at 600 MHz. [e]Recorded at 100 MHz. [f]Recorded at 150 MHz. "m" means overlapped or multiplet with other signals.

brane domain of P-gp, which is lined by residues Ser-728, Phe-727, Gln-724, Leu-723, Phe-335, Leu-338, Ile-339, Phe-324, Ala-301, Phe-302, Ile-305, Tyr-306, Ser-308, and Tyr-309. Additionally, several hydrogen bonding interactions with the side chains of Gln-724 and Tyr-306 were observed. In conclusion, based on substantial favorable biological data, **1** exhibits potential for use in combination with conventional chemotherapies in the treatment of cancers affected by P-gp-mediated MDR.

3. Discussion

This study reports the isolation of seven previously undescribed eremophilane-type sesquiterpenoids and *nor*-sesquiterpenoids (**1**–**5** and **7**–**8**), a previously undescribed eudesmane-type sesquiterpenoid (**9**), and four known compounds (**6** and **10**–**12**) from fungus *P. roqueforti*. Notably, compounds **1**–**3** represent rare examples of 11,12,13-tri-*nor*-sesquiterpenoids with a 6/6 bicyclic core, while compound **4** is an unusual 7,11,12,13-tetra-*nor*-sesquiterpenoid, featuring an oxabicyclo-[4.4.0]-nonane skeleton. In the bioassay, all twelve compounds were evaluated for the anti-MDR cancer activity in SW620/Ad300 cells. The results indicate that compound **1** in combination with PTX demonstrated significantly higher efficacy (IC_{50} 50.36 nmol·L^{-1}) in SW620/Ad300 cells compared to PTX alone (IC_{50} 3.26 μmol·L^{-1}). These findings suggest that this study may provide a new chemical lead for the development of agents to overcome MDR cancer.

4. Experimental

4.1. General experimental procedures

Optical rotations were measured using a Perkin-Elmer 341 spectropolarimeter in MeOH. Ultra violet (UV) spectra were obtained in MeOH with a Lambda 35 instrument. IR spectra were recorded using a Vertex 70 FT-IR spectrophotometer. ECD data were collected on a JASCO-810 spectrometer. HR-ESI-MS data were acquired from a Bruker MicrOTOF II spectrometer. 1D & 2D NMR spectra were recorded on a Bruker AM-400 or AM-600 spectrometer. The chemical shifts (δ) were expressed in ppm relative to the solvent signals for methanol-d_4 (δ_H 3.31 and δ_C 49.0) and chloroform-d (δ_H 7.26 and δ_C77.2). Semi-preparative high performance liquid chromatography (HPLC) was conducted using an Agilent HPLC system with a reversed-phase (RP) C_{18} column (10 mm × 250 mm). Column chromatography (CC) was performed on ODS (50 μm), silica gel (200–300, 100–200, and 80–120 meshes; Qingdao Marine Chemical Inc., Qingdao, China), and Sephadex LH-20. Fractions were monitored by thin-layer chromatography (TLC), and spots were visualized by heating silica gel plates sprayed with 10% H_2SO_4 in EtOH.

4.2. Fungal material

The strain *P. roqueforti* was isolated from the root soil of *Hypericum beanii*, collected in Shennongjia Forestry District, Hubei Province, China, during August 2018. Authentication of this strain was conducted based on morphological characteristics and sequence analysis of the ITS region of rDNA. The sequence data for this strain have been deposited in GenBank under the accession number ON795101. The fungus is currently preserved in the culture collection of the College of Pharmacy, Tongji Medical College, Huazhong University of Science and Technology.

4.3. Extraction and isolation

The fungal strain was cultivated on potato dextrose agar (PDA) at 26 °C to prepare the seed cultures. Subsequently, the agar plugs were sectioned into small pieces and inoculated into 240 Erlenmeyer flasks (1 L), each containing 250 g of rice and 180 mL of distilled water, sterilized by autoclave. Following incubation at 26 °C for 30 d, the fermented rice substrate underwent extraction with 95% aqueous EtOH seven times. The organic solvents were evaporated under vacuum to yield an extract (358 g), which was fractionated by silica gel CC eluted with petroleum ether (PE)–ethyl acetate (EtOAc) gradient system

Table 3 Inhibition ratios (%) of **1**–**12** (20 μmol·L^{-1}) to several cancer and MDR cells

Compound	Cancer cells			MDR cells	
	MCF7	HepG2	C4-2B	SW620/Ad300	SW620/Ad300 (with PTX)
1	9.05 ± 2.00	6.45 ± 1.61	12.04 ± 1.22	2.64 ± 0.95	81.12 ± 1.81
2	63.57 ± 1.68	11.00 ± 1.36	17.28 ± 1.21	83.79 ± 0.04	-
3	3.83 ± 1.76	15.90 ± 2.71	23.98 ± 1.27	15.10 ± 1.34	18.92 ± 1.97
4	1.29 ± 1.22	6.90 ± 3.34	15.22 ± 0.17	7.98 ± 1.19	6.90 ± 1.03
5	0.33 ± 0.06	6.64 ± 1.05	15.90 ± 1.22	0.95 ± 0.18	7.06 ± 0.79
6	1.07 ± 0.14	6.30 ± 1.33	1.47 ± 0.75	3.03 ± 0.12	8.10 ± 0.37
7	13.54 ± 2.33	14.10 ± 2.27	11.10 ± 1.22	3.34 ± 0.61	2.80 ± 0.05
8	1.50 ± 0.33	9.53 ± 3.10	16.97 ± 1.73	12.80 ± 0.68	10.40 ± 0.62
9	2.84 ± 0.35	6.67 ± 1.04	11.31 ± 0.58	17.28 ± 1.69	12.97 ± 1.28
10	3.38 ± 0.84	2.79 ± 0.29	16.03 ± 1.44	2.69 ± 0.43	13.90 ± 1.18
11	12.60 ± 1.29	9.40 ± 1.65	13.40 ± 0.51	2.58 ± 0.38	17.63 ± 0.65
12	12.20 ± 6.64	12.70 ± 1.02	11.50 ± 0.60	16.80 ± 3.20	10.54 ± 1.03

"-": no tested.

(30∶1→0∶1) to obtain six main fractions (A–F) based on TLC analyses. Fraction D (9.8 g) was isolated by RP-C_{18} silica gel CC eluted with MeOH–H_2O (20%, 40%, 60%, 80%, and 100%) to afford four main fractions (D1–D4). Fraction D3 (1.6 g) was subjected to silica gel CC (PE–EtOAc, 10∶1–1∶1, *V*/*V*) to afford four main subfractions (D3-1–D3-4). Subfraction D3-3 (275 mg) was separated by repeated semi-preparative RP-C_{18} HPLC (MeCN–H_2O, 50∶50, *V*/*V*; 2.0 mL·min^{-1}) to afford compounds **10** (8.6 mg, t_R = 27 min), **11** (22.5 mg, t_R = 35 min), and **12** (9.4 mg, t_R = 59 min). Fraction E (11.3 g) was chromatographed over ODS (MeOH–H_2O, 20%–100%) to yield five main subfractions (E1–E5). Subfraction E4 (376 mg) was separated by Sephadex LH-20 CC eluted with CH_2Cl_2–MeOH (1∶1, *V*/*V*), and further purified by RP HPLC (MeCN–H_2O, 55∶45, *V*/*V*; 2.0 mL·min^{-1}) to yield compounds **8** (4.4 mg, t_R = 11 min) and **9** (15.2 mg, t_R = 16 min). Subfraction E5 (853 mg) was separated by Sephadex LH-20 CC eluted with CH_2Cl_2–MeOH (1∶1, *V*/*V*), and further purified by RP HPLC (MeCN–H_2O, 35∶65, *V*/*V*; 2.0 mL·min^{-1}) to yield compounds **2** (5.2 mg, t_R = 16 min), **3** (10.0 mg, t_R = 35 min), **4** (4.1 mg, t_R = 31 min), **6** (3.0 mg, t_R = 50 min), and **7** (2.8 mg, t_R = 18 min). Fraction F (5.6 g) was chromatographed over ODS (MeOH–H_2O, 20%–100%) to yield five main subfractions (F1–F5). Subfraction F2 (155 mg) was separated by Sephadex LH-20 CC eluted with CH_2Cl_2–MeOH (1∶1, *V*/*V*), and further purified by RP HPLC (MeCN–H_2O, 42∶58, *V*/*V*; 2.0 mL·min^{-1}) to yield compounds **1** (8.2 mg, t_R = 33 min) and **5** (2.0 mg, t_R = 16 min).

Peniroqueforin E ***(1)***: yellow needle crystals; $[\alpha]_D^{25}$: +193 (*c* 0.10, MeOH); UV (MeOH) λ_{max} (log ε) 221 (4.03), 277 (4.00) nm; ECD (MeOH) (Δε) 221 (+11.95), 242 (+0.92), 275 (+4.89), 315 (–0.59) nm; IR ν_{max} 3294, 2992, 1737, 1638, 1627, 1423, 1373, 1240, 1220, 986, 910, 650 cm^{-1}; HR-ESI-MS *m*/*z* 271.0940 [M + Na]$^+$ (Calcd. for $C_{14}H_{16}O_4Na^+$, 271.0941); ^{1}H and ^{13}C NMR data, see Table 1.

Peniroqueforin F ***(2)***: yellow amorphous powder; $[\alpha]_D^{25}$: +168 (*c* 0.10, MeOH); UV (MeOH) λ_{max} (log ε) 206 (3.74), 242 (3.95), 289 (3.96) nm; ECD (MeOH) (Δε) 209 (–8.68), 239 (+17.79), 263 (+2.96), 284 (+8.53), 328 (–2.93) nm; IR ν_{max} 3383, 2921, 2851, 1676, 1633, 1419, 1386, 1299, 1222, 1199, 912, 899, 645 cm^{-1}; HR-ESI-MS *m*/*z* 227.0688 [M + Na]$^+$ (Calcd. for $C_{12}H_{12}O_3Na^+$, 227.0679); ^{1}H and ^{13}C NMR data, see Table 1.

Peniroqueforin G ***(3)***: yellow needle crystals; $[\alpha]_D^{25}$: +138 (*c* 0.10, MeOH); UV (MeOH) λ_{max} (log ε) 206 (3.94), 253 (3.90) nm; ECD (MeOH) (Δε) 200 (+3.74), 252 (–3.57), 327 (+0.42) nm; IR ν_{max} 3354, 2957, 2850, 1723, 1646, 1375, 1251, 1229, 1168, 1122, 903, 878, 691 cm^{-1}; HR-ESI-MS *m*/*z* 287.0891 [M + Na]$^+$ (Calcd. for $C_{14}H_{16}O_5Na^+$, 287.0890); ^{1}H and ^{13}C NMR data, see Table 1.

Peniroqueforin H ***(4)***: yellow block crystals; $[\alpha]_D^{25}$: +152 (*c* 0.10, MeOH); UV (MeOH) λ_{max} (log ε) 264 (4.10) nm; ECD (MeOH) (Δε) 272 (+16.67) nm; IR ν_{max} 3273, 2921, 2851, 1744, 1667, 1635, 1247, 1231, 1093, 973, 907, 881, 725, 676, 574 cm^{-1}; HR-ESI-MS *m*/*z* 253.1068 [M + H]$^+$ (Calcd. for $C_{13}H_{16}O_5H^+$, 253.1071); ^{1}H and ^{13}C NMR data, see Table 1.

Peniroqueforin I ***(5)***: yellow block crystals; $[\alpha]_D^{25}$: +96 (*c* 0.10, MeOH); UV (MeOH) λ_{max} (log ε) 202 (4.36), 251 (3.78) nm; ECD (MeOH) (Δε) 209 (+5.26), 244 (+9.50), 285 (–2.43) nm; IR ν_{max} 3395, 2921, 2851, 1658, 1628, 1439, 1370, 1298, 1228, 1081, 1038, 945, 887, 720, 650 cm^{-1}; HR-ESI-MS *m*/*z* 273.1461 [M + Na]$^+$ (Calcd. for $C_{15}H_{22}O_3Na^+$, 273.1461); ^{1}H and ^{13}C NMR data, see Table 2.

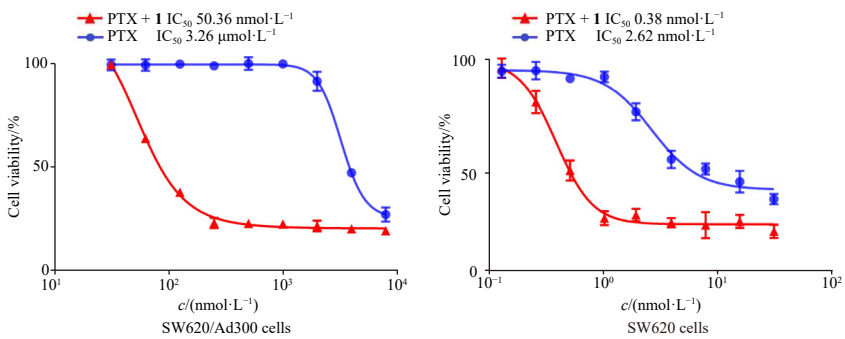

Fig. 6 Compound **1** effected the cell viability of SW620/Ad300 cells (left) and SW620 cells (right) with the combination of PTX. Data are presented as the mean ± SD (*n* = 5).

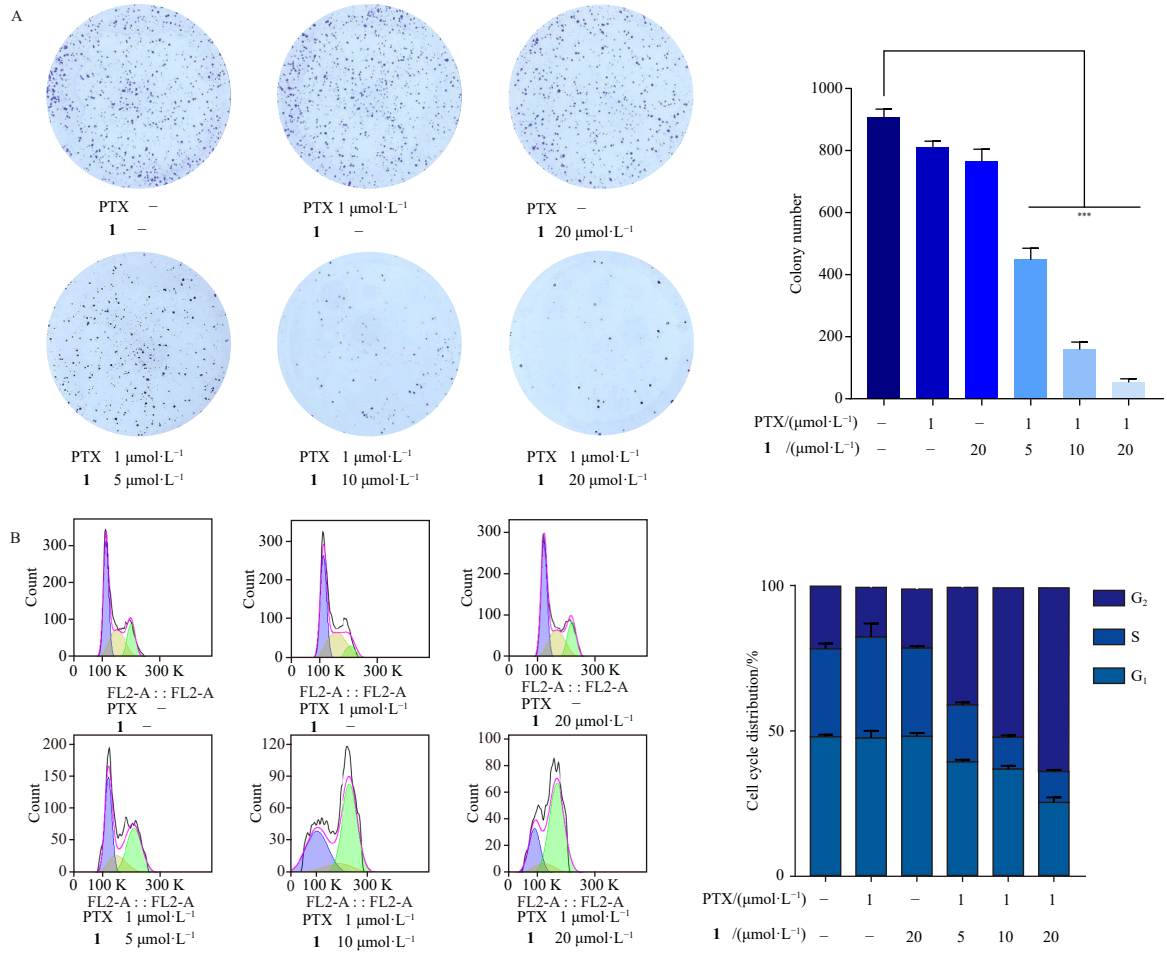

Fig. 7 Compound **1** inhibited the colony formation and cell cycle of SW620/Ad300 cells with the combination of PTX. (A) The colony formation of SW620/Ad300 cells treated with 1 or PTX or their combination. (B) The cell cycle analysis of SW620/Ad300 cells treated with 1 or PTX or their combination. Data are presented as the mean ± SD (n = 3). $^{***}P < 0.001$ *vs* NC.

Peniroqueforin J (***7***): yellow amorphous powder; $[\alpha]_D^{25}$: −51 (*c* 0.10, MeOH); UV (MeOH) λ_{max} (log ε) 202 (3.80), 243 (3.60) nm; ECD (MeOH) ($\Delta\varepsilon$) 219 (+1.43), 246 (+4.60), 285 (−0.71) nm; IR ν_{max} 3439, 2973, 2939, 1739, 1694, 1659, 1383, 1243, 1090, 1025, 986, 948, 900, 663, 635, 590 cm^{-1}; HR-ESI-MS *m/z* 315.1206 $[M + Na]^+$ (Calcd. for $C_{16}H_{20}O_5Na^+$, 315.1203); ^1H and ^{13}C NMR data, see Table 2.

Peniroqueforin K (***8***): yellow amorphous powder; $[\alpha]_D^{25}$: +168 (*c* 0.10, MeOH); UV (MeOH) λ_{max} (log ε) 204 (3.67), 250 (3.58) nm; ECD (MeOH) ($\Delta\varepsilon$) 246 (+12.72), 285 (−4.84) nm; IR ν_{max} 3367, 2922, 2873, 1660, 1628, 1462, 1371, 1299, 1226, 1168, 1071, 1020, 904, 720, 661, 618 cm^{-1}; HR-ESI-MS *m/z* 273.1467 $[M + Na]^+$ (Calcd. for $C_{15}H_{22}O_3Na^+$, 273.1461). For ^1H and ^{13}C NMR data, see Table 2.

Peniroqueforin L (***9***): colorless oil; $[\alpha]_D^{25}$: +252 (*c* 0.10, MeOH); UV (MeOH) λ_{max} (log ε) 241 (3.96) nm; ECD (MeOH) ($\Delta\varepsilon$) 241 (+2.85), 327 (−0.29) nm; IR ν_{max} 3422, 3366, 2967, 2921, 1663, 1378, 1261, 1045, 1026, 891, 720, 629, 593, 548 cm^{-1}; HR-ESI-MS *m/z* 235.1692 $[M + H]^+$ (Calcd. for $C_{15}H_{22}O_2H^+$, 235.1693). For ^1H and ^{13}C NMR data, see Table 2.

4.4. X-ray crystal structure analysis

Crystals of compounds **1** and **3**–**5** were obtained from MeOH–H_2O (20∶1, *V*/*V*) at 4 °C. Intensity data were collected using a XtaLAB PRO MM007HF diffractometer with Cu Kαradiation. The structures were solved by direct methods in Olex2 [27] using SHELXL-2014/7 [28]. Refinements were performed using the SHELXL-2014/7 refinement package *via* full-matrix least-squares on F^2, employing anisotropic displacement parameters for all non-hydrogen atoms. Hydrogen atoms were positioned at calculated locations and refined using a riding model. Crystallographic data for these structures have been deposited in the CCDC (CCDC 2304403 for **1**, CCDC 2304404 for **3**, CCDC 2304405 for **4**, and CCDC 2304406 for **5**). Copies of the data can be obtained free of charge by application to CCDC, 12 Union Road, Cambridge CB 1EZ, UK [fax: Int. + 44 (0) (1223) 336 033; e-mail: deposi@ccdc.cam.ac.uk].

Crystallographic data for compound ***1***: $C_{14}H_{16}O_4$, M = 248.27, a = 6.0289 (5) Å, b = 11.4601(10) Å, c = 17.7853(16) Å, α = 90°, β = 90°, γ = 90°, V = 1228.82(18) $Å^3$, T = 150(2) K, space group $P2_12_12_1$, Z = 4, μ(Cu Kα) = 0.809 mm^{-1}, 8698 reflections measured, 2257 independent reflections (R_{int} = 0.0437). The final R_1 values were 0.0284 ($I > 2\sigma(I)$). The final $wR(F^2)$ values were 0.0782 ($I > 2\sigma(I)$). The final R_1 values were 0.0302 (all data). The final $wR(F^2)$ values were 0.0792 (all data). The goodness of fit on F^2 was 1.064. Flack parameter = 0.13(7) (CCDC 2304403).

Crystallographic data for compound ***3***: $C_{14}H_{16}O_5$, M = 264.27, a = 7.2855(2) Å, b = 9.3935(3) Å, c = 9.8352(3) Å, α = 105.4200(10)°, β = 99.4900(10)°, γ = 90.2810(10)°, V = 636.44(3) $Å^3$, T = 150(2) K, space group $P1$, Z = 2, μ(Cu Kα) = 0.876 mm^{-1}, 16718 reflections measured, 4705 independent reflections (R_{int} = 0.0591). The final R_1 values were 0.0374 ($I > 2\sigma(I)$). The final $wR(F^2)$ values were 0.1016 ($I > 2\sigma(I)$). The final R_1 values were 0.0398 (all data). The final $wR(F^2)$ values were 0.1033 (all data). The goodness of fit on F^2 was 1.088. Flack parameter = 0.12(8) (CCDC 2304404).

Crystallographic data for compound ***4***: $C_{13}H_{16}O_5$, M = 252.26,

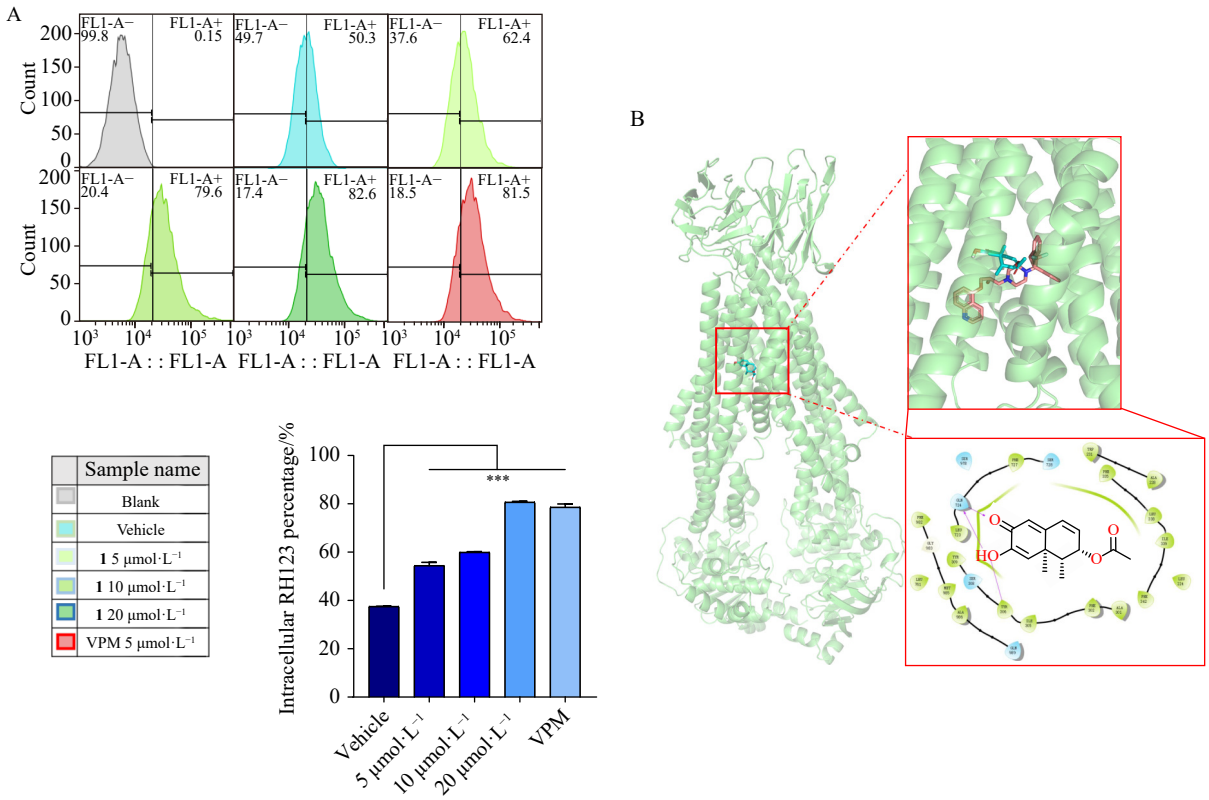

Fig. 8 Compound **1** effected the transport capacity of P-gp. (A) The fluorescence intensity of Rhodamine 123 in SW620/Ad300 cells and the intracellular Rhodamine 123 percentage with 30 min treated by **1**. (B) The ribbon diagram of P-gp with the binding location of **1** at the internal cavity and the 2D bonding interaction of **1** within P-gp. Data are presented as the mean ± SD (n = 3), $^{***}P < 0.001$ *vs* NC.

a = 8.74300(10) Å, b = 8.18980(10) Å, c = 9.2572(2) Å, α = 90°, β = 111.314(2)°, γ = 90°, V = 617.510(19) Å^3, T = 293(2) K, space group $P2_1$, Z = 2, μ(Cu Kα) = 0.874 mm^{-1}, 5463 reflections measured, 2395 independent reflections (R_{int} = 0.0220). The final R_1 values were 0.0339 ($I > 2\sigma(I)$). The final $wR(F_2)$ values were 0.0909 ($I > 2\sigma(I)$). The final R_1 values were 0.0346 (all data). The final $wR(F_2)$ values were 0.0915 (all data). The goodness of fit on F_2 was 1.063. Flack parameter = 0.14(10) (CCDC 2304405).

Crystallographic data for compound ***5***: $C_{15}H_{22}O_3 \bullet H_2O$, M = 268.34, a = 10.3376(3) Å, b = 10.8860(4) Å, c = 12.5015(4) Å, α = 90°, β = 90°, γ = 90°, V = 1406.86(8) Å^3, T = 150(2) K, space group $P2_12_12_1$, Z = 4, μ(Cu Kα) = 0.734 mm^{-1}, 11687 reflections measured, 2678 independent reflections (R_{int} = 0.0550). The final R_1 values were 0.0413 ($I > 2\sigma(I)$). The final $wR(F_2)$ values were 0.1099 ($I > 2\sigma(I)$). The final R_1 values were 0.0430 (all data). The final $wR(F_2)$ values were 0.1109 (all data). The goodness of fit on F_2 was 1.116. Flack parameter = 0.07(7) (CCDC 2304406).

4.5. ECD calculation

Conformational analyses were conducted through random searching in Sybyl-X 2.0, utilizing the MMFF94S force field with an energy cutoff of 5 kcal·mol^{-1}. The analysis revealed six lowest energy conformers for **9**. Subsequently, geometry optimizations and frequency analyses were performed at the B3LYP-D3(BJ)/6-31G* level in CPCM methanol using ORCA5.0.1[29–30]. All conformers employed for property calculations in this study were confirmed as stable points on the potential energy surface (PES) with no imaginary frequencies. The excitation energies, oscillator strengths, and rotational strengths (velocity) of the first 60 excited states were calculated using TD-DFT methodology at the PBE0/def2-TZVP level in CPCM methanol using ORCA5.0.1. The ECD spectra were simulated using the overlapping Gaussian function (half the bandwidth at 1/e peak height, sigma = 0.30 for all). Gibbs free energies for conformers were determined using thermal correction at the B3LYP-D3(BJ)/6-31G* level and electronic energies evaluated at the wB97M-V/def2-TZVP level in CPCM methanol using ORCA5.0.1. To obtain the final spectra, the simulated spectra of the conformers were averaged according to the Boltzmann distribution theory and their relative Gibbs free energy (ΔG). The absolute configuration of **9** was determined by comparing the experimental spectrum with the calculated model molecules.

4.6. Cell lines and reagents

The MDR human colon cancer cell line SW620/Ad300 was provided by Professor Hongmin Liu (Department of Oncology, the Affiliated Cancer Hospital of Zhengzhou University, Zhengzhou, China). Cells were cultured in Dulbecco's modified Eagle's medium (DMEM) supplemented with 10% fetal bovine serum (Procell Life Science & Technology, Wuhan, China), 100 U·mL^{-1} penicillin, and 100 μg·mL^{-1} streptomycin. The cells were maintained in an incubator at 37 °C with 5% CO_2.

4.7. Cell counting kit-8 (CCK-8) assay

The CCK-8 assay was employed to assess the cytotoxicity of the compounds. Cells were seeded into 96-well microplates and cultured overnight. Following 72 h of incubation with various concentrations of compounds, the used medium was aspirated and replaced with 100 μL of fresh medium containing CCK-8 (100 μL·mL^{-1}). The 96-well microplate was then incubated in darkness for 2 h. Absorbance measurements for each well were taken at 450 nm using a Varioskan LUX microplate spectrophotometer (Thermo Fisher, Waltham, MA). IC_{50} values were calculated using GraphPad Prism software.

4.8. Colony formation assay

SW620/Ad300 cells were seeded into 6-well plates (2000 cells/well) and cultured overnight. The cells were then treated

with the compound (20 μmol·L^{-1}), PTX (1 μmol·L^{-1}), or a combination of both for 7 days. Subsequently, the medium was removed, and the plates were washed with phosphate buffered saline (PBS). Cells were fixed with 4% paraformaldehyde (Biossci, Wuhan, China) and stained with 0.1% (*W/V*) crystal violet staining solution (Biosharp, Beijing, China) for 30 minutes. Finally, the plates were washed with ultrapure water and air-dried.

4.9. Cell cycle analysis

SW620/Ad300 cells were seeded into 6-well plates and cultured overnight. The cells were then treated with compounds (20 μmol·L^{-1}), PTX (1 μmol·L^{-1}), or a combination of both. After 24 h, the treated cells were collected and washed twice with PBS. Subsequently, the cells were fixed with 70% ethanol at –20 °C overnight. Following ethanol removal and PBS washing, the cells were stained with propidium iodide solution containing RNase A using the Cell Cycle and Apoptosis Analysis Kit (Beyotime, Shanghai, China). Cell cycle progression was analyzed using a BD FACS flow cytometer.

4.10. Rho 123 accumulation assay

SW620/Ad300 cells were seeded in 6-well plates and cultured overnight to ensure proper adhesion. Subsequently, the cells were treated with compounds at a concentration of 20 μmol·L^{-1} for 24 h. Following treatment, the cells were incubated with 5 μg·mL^{-1} of Rho 123 for 30 min at 37 °C. After incubation, excess dye was removed by washing the cells twice with ice-cold PBS. Finally, the cells were resuspended in PBS and analyzed using a BD FACS flow cytometer.

Funding

This work was supported by the National Natural Science Foundation of China (Nos. 82273811, 32470417, and U22A20380), the National Program for Support of Top-notch Young Professionals (No. 0106514050), the Hubei Provincial Natural Science Foundationof China (No. 2024AFA028), the National Key R & D Program of China (No. 2021YFA0910500), the Science and Technology Major Project of Hubei Province (Nos. 2021ACA012 and 2024BCB021), and the Chinese Medicine Research Foundation of the Health Commission of Hubei Province (No. ZY2025Z013).

Supporting Information

Supporting information of this paper can be requested by sending E-mail to the corresponding authors.

Declaration of competing interest

These authors have no conflict of interest to declare.

References

1 Wang JQ, Li JY, Teng QX, et al. Venetoclax, a BCL-2 inhibitor, enhances the efficacy of chemotherapeutic agents in wild-type ABCG2-overexpression mediated MDR cancer cells. *Cancers*. 2020;12(2):466. https://doi.org/10.3390/cancers12020466.
2 Shi RC, Tang YQ, Miao HM. Metabolism in tumor microenvironment: implications for cancer immunotherapy. *MedComm*. 2020;1(1):47-68. https://doi.org/10.1002/mco2.6.
3 Mo SY, Zhao ZM, Ye Z, et al. New secondary metabolites with cytotoxicity from fungus *Penicillium roqueforti*. *Nat Prod Bioprospect*, 2023;13(1):17. https://doi.org/10.1007/s13659-023-00381-4.
4 Krishna R, Mayer LD. Multidrug resistance (MDR) in cancer. Mechanisms, reversal using modulators of MDR and the role of MDR modulators in influencing the pharmacokinetics of anticancer drugs. *Eur J Pharm Sci*. 2000;11(4):265-283. https://doi.org/10.1016/s0928-0987(00)00114-7.
5 Omran Z, Scaife P, Stewart S, et al. Physical and biological characteristics of multi drug resistance (MDR): an integral approach considering pH and drug resistance in cancer. *Semin Cancer Biol*. 2017;43:42-48. https://doi.org/10.1016/j.semcancer.2017.01.002.
6 Wang MC, Liang LL, Wang, R, et al. Narciclasine, a novel topoisomerase I inhibitor, exhibited potent anti-cancer activity against cancer cells. *Nat Prod Bioprospect*. 2023;13:27. https://doi.org/10.1007/s13659-023-00392-1.
7 Bailly C, Vergoten G. Anticancer properties and mechanism of action of oblongifolin C, guttiferone K and related polyprenylated acylphloroglucinols. *Nat Prod Bioprospect*. 2021;11(6):629-641. https://doi.org/10.1007/s13659-021-00320-1.
8 Joshi P, Vishwakarma RA, Bharate SB. Natural alkaloids as P-gp inhibitors for multidrug resistance reversal in cancer. *Eur J Med Chem*. 2017;138:273-292. https://doi.org/10.1016/j.ejmech.2017.06.047.
9 Fang LY, Zhang GS, Li CL, et al. Discovery of a daunorubicin analogue that exhibits potent antitumor activity and overcomes P-gp-mediated drug resistance. *J Med Chem*. 2006;49(3):932-941. https://doi.org/10.1021/jm050800q.
10 Du WY, Yang Q, Xu HM, et al. Drimane-type sesquiterpenoids from fungi. *Chin J Nat Med*. 2022;20(10): 737-748. https://doi.org/10.1016/S1875-5364(22)60190-0.
11 Li W, Wei J, Chen DY, et al. Study on the secondary metabolites of grasshopper-derived fungi *Arthrinium* sp. NF2410. *Chin J Nat Med*. 2020;18(1): 77-80. https://doi.org/10.1016/S1875-5364(20)60040-1.
12 Mo SY, Yin J, Ye Z, et al. Asperanstinoids A–E: undescribed 3,5-dimethylorsellinic acid-based meroterpenoids from *Aspergillus calidoustus*. *Phytochemistry*. 2021;190:112892. https://doi.org/10.1016/j.phytochem.2021.112892.
13 Li Y, Jian YJ, Xu F, et al. Five new terpenoids from *Viburnum odoratissimum* var. *sessiliflorum*. *Chin J Nat Med*. 2023;21(4):298-307. https://doi.org/10.1016/S1875-5364(23)60438-8.
14 Yan LH, Li PH, Li XM, et al. Bialorastins A–F, highly oxygenated and polycyclic andrastin-type meroterpenoids with proangiogenic activity from the deep-sea cold-seep-derived fungus *Penicillium bialowiezense* CS-283. *Bioorg Chem*. 2024;143:107073. https://doi.org/10.1016/j.bioorg.2023.107073.
15 Xu JQ, Hu LH. Five new eremophilane sesquiterpenes from *Ligularia przewalskii*. *Helv Chim Acta*. 2008;91:951-957. https://doi.org/10.1002/hlca.200890101.
16 Lin LB, Xiao J, Gao YQ, et al. Trinor- and tetranor-eremophilane sesquiterpenoids with anti-neuroinflammatory activity from cultures of the fungus *Septoria rudbeckiae*. *Phytochemistry*. 2021;183:112642. https://doi.org/10.1016/j.phytochem.2020.112642.
17 Zhao Y, Peng H, Jia ZJ. Six new eremophilane derivatives from two *ligularia* species. *J Nat Prod*. 1994;57(12):1626-1630. https://doi.org/10.1021/np50114a003.
18 Wang A, Yin RY, Zhou ZY, et al. Eremophilane-type sesquiterpenoids from the endophytic fungus *Rhizopycnis vagum* and their antibacterial, cytotoxic, and phytotoxic activities. *Front Chem*. 2020;8:596889. https://doi.org/10.3389/fchem.2020.596889.
19 O'Donnell TJ, Luo YH, Yoshida WY, et al. Spirovetivane- and eudesmane-type sesquiterpenoids isolated from the culture media of two cyanobacterial strains. *J Nat Prod*. 2022;85(2):415-425. https://doi.org/10.1021/acs.jnatprod.1c01014.
20 Sun YL, Gerke J, Becker K, et al. Rapid discovery of terpene tailoring enzymes for total biosynthesis. *Chem Sci*. 2023;14(45):13463-13467. https://doi.org/10.1039/d3sc04172g.
21 Le DH, Takenaka Y, Hamada N, et al. Eremophilane-type sesquiterpenes from cultured lichen mycobionts of *Sarcographa tricosa*. *Phytochemistry*. 2013;91:242-248. https://doi.org/10.1016/j.phytochem.2012.01.009.
22 Castro SJ, Garcia ME, Padrón JM, et al. Phytochemical study of *Senecio volckmannii* assisted by CASE-3D with residual dipolar couplings and isotropic $^{1}H/^{13}C$ NMR chemical shifts. *J Nat Prod*. 2018;81(11):2329-2337. https://doi.org/10.1021/acs.jnatprod.8b00162.
23 Saito Y, Ichihara M, Okamoto Y, et al. Four new eremophilane-type alcohols from *Cremanthodium Helianthus* collected in China. *Nat Prod Commun*. 2012;7(4):423-426. https://doi.org/10.1177/1934578X1200700402.
24 Wang S, Wang SQ, Teng QX, et al. Structure-based design, synthesis, and biological evaluation of new triazolo[1,5-*a*] pyrimidine derivatives as highly potent and orally active ABCB1 modulators. *J Med Chem*. 2020;63(24):15979-15996. https://doi.org/10.1021/acs.jmedchem.0c01741.
25 Yang ZK, Cai Y, Yang X, et al. Novel benzo five-membered heterocycle derivatives as P-glycoprotein inhibitors: design, synthesis, molecular docking, and anti-multidrug resistance activity. *J Med Chem*. 2023;66(8):5550-5556. https://doi.org/10.1021/acs.jmedchem.2c01999.
26 Wang SQ, Teng QX, Wang S, et al. Preclinical studies of the triazolo[1,5-*a*] pyrimidine derivative WS-716 as a highly potent, specific and orally active P-glycoprotein (P-gp) inhibitor. *Acta Pharm Sin B*. 2022;12(8):3263-3280. https://doi.org/10.1016/j.apsb.2022.03.023.
27 Hubschle CB, Sheldrick GM, Dittrich B. ShelXle: a Qt graphical user interface for SHELXL. *J Appl Crystallogr*. 2011;44(Pt 6):1281-1284. https://doi.org/10.1107/S0021889811043202.
28 Sheldrick G. Phase annealing in SHELX-90: direct methods for larger structures. *Acta Cryst A*. 1990;46:467-473. https://doi.org/10.1107/S0108767390000277.
29 Neese F. The ORCA program system. *Wiley Interdiscip Rev Comput Mol Sci*. 2012;2(1):73-78. https://doi.org/10.1002/wcms.81.
30 Stephens PJ, Harada N. ECD cotton effect approximated by the Gaussian curve and other methods. *Chirality*. 2010;22(2):229-233. https://doi.org/10.1002/chir.20733.